Title

Ileal interposition surgery targets the hepatic TGF-β pathway, influencing gluconeogenesis and mitochondrial bioenergetics in the UCD-T2DM rat model of diabetes

Journal

The FASEB Journal, 33(10)

ISSN

0892-6638

Authors

Hung, Connie
Napoli, Eleonora
Ross-Inta, Catherine
et al.

Publication Date

2019-10-01

DOI

10.1096/fj.201802714r

Peer reviewed

THE FASEB JOURNAL • RESEARCH • www.fasebj.org

Ileal interposition surgery targets the hepatic TGF-β pathway, influencing gluconeogenesis and mitochondrial bioenergetics in the UCD-T2DM rat model of diabetes

Connie Hung,* Eleonora Napoli,* Catherine Ross-Inta,* James Graham,† Amanda L. Flores-Torres,*,‡ Kimber L. Stanhope,*,† Pascal Froment,§ Peter J. Havel,*,† and Cecilia Giulivi*,¶,1

*Department of Molecular Biosciences, School of Veterinary Medicine, †Department of Nutrition, and ¶Medical Investigations of Neurodevelopmental Disorders (MIND) Institute, University of California, Davis, Davis, California, USA; ‡Department of Biochemistry, Medical Sciences Campus, University of Puerto Rico, San Juan, Puerto Rico; and §Unité de Physiologie de la Reproduction et des Comportements, Institut National de la Recherche Agronomique, Unité Mixte de Recherche (UMR) 85, Paris, France

ABSTRACT: Ileal interposition (IT) is a surgical procedure that increases the delivery of incompletely digested nutrients and biliary and pancreatic secretions to the distal intestinal mucosa. Here, we investigated the metabolic impact of this intervention in 2-mo-old prediabetic University of California, Davis type 2 diabetes mellitus rats by assessing liver gene expression at 1.5 mo post-IT surgery. Pathway analysis indicated decreased signaling *via* TGF-β/Smad (a family of proteins named mothers against decapentaplegic homologs), peroxisome proliferator-activated receptor (PPAR), and PI3K-Akt-AMPK–mechanistic target of rapamycin, likely targeting hepatic stellate cells because differentiation and activation of these cells is associated with decreased signaling *via* PPAR and TGF-β/Smad. IT surgery up-regulated the expression of genes involved in regulation of cholesterol and terpenoid syntheses and down-regulated those involved in glycerophospholipid metabolism [including cardiolipin (CL)], lipogenesis, and gluconeogenesis. Consistent with the down-regulation of the hepatic CL pathway, IT surgery produced a metabolic switch in liver, kidney cortex, and fat depots toward decreased mitochondrial fatty acid β-oxidation, the process required to fuel high energy–demanding pathways (*e.g.*, gluconeogenesis and glyceroneogenesis), whereas opposite effects were observed in skeletal and cardiac muscles. This study demonstrates for the first time the presence of metabolic pathways that complement the effects of IT surgery to maximize its benefits and potentially identify similarly effective, durable, and less invasive therapeutic options for metabolic disease, including inhibitors of TGF-β signaling.—Hung, C., Napoli, E., Ross-Inta, C., Graham, J., Flores-Torres, A. L., Stanhope, K. L., Froment, P., Havel, P. J., Giulivi, C. Ileal interposition surgery targets the hepatic TGF-β pathway, influencing gluconeogenesis and mitochondrial bioenergetics in the UCD-T2DM rat model of diabetes. FASEB J. 33, 000–000 (2019). www.fasebj.org

KEY WORDS: IT surgery · metabolomics · type 2 diabetes mellitus

Type 2 diabetes mellitus (T2DM) is a devastating metabolic disease with an increasing worldwide burden, resulting in a critical need for new effective preventive and therapeutic strategies. In the U.S. alone, an estimated 30.3 million people of all ages—or 9.4% of the population—had diabetes in 2015 (1). This total included 30.2 million adults aged 18 yr or older (12.2% of all U.S. adults), of which 7.2 million (23.8%) were not aware of having diabetes (1). If not managed effectively, diabetes can ensue in a multisystemic disorder (*e.g.*, affecting the cardiovascular system, eyes, kidneys, nerves, gums, and teeth), making it the leading cause of adult blindness, kidney failure, and nontraumatic lower-limb amputations. Poorly controlled

ABBREVIATIONS: AdipoR, adiponectin receptor; CCO, cytochrome C oxidase; CL, cardiolipin; CRLS1, CL synthase 1; CS, citrate synthase; CYP7A1, cholesterol 7α-hydroxylase; FAO, fatty acid β-oxidation; FC, fold change; Fox, forkhead box; HSC, hepatic stellate cell; IT, ileal interposition; mTOR, mechanistic target of rapamycin; NQR, NADH-decylubiquinone oxidoreductase; oxphos, oxidative phosphorylation; PPAR, peroxisome proliferator-activated receptor; qRT-PCR, quantitative RT-PCR; SCCR, succinate-cytochrome *c* reductase; T2DM, type 2 diabetes mellitus; TAG, triacylglyceride; UCD, University of California, Davis

[1] Correspondence: Department of Molecular Biosciences, University of California, Davis, 1089 Veterinary Dr., 3017 VetMed3B, Davis, CA 95616, USA. E-mail: cgiulivi@ucdavis.edu

doi: 10.1096/fj.201802714R
This article includes supplemental data. Please visit *http://www.fasebj.org* to obtain this information.

diabetes also increases the risk for cardiovascular diseases including stroke and myocardial infarction (1–3). With the increased worldwide prevalence of T2DM, the development of therapeutic strategies to prevent or delay diabetes onset in predisposed individuals has become critical. Delaying the age of onset of diabetes by even a few years, will postpone the development of the devastating complications of diabetes (including retinopathy, kidney failure/dialysis, and limb amputation) reducing patient suffering and generating a massive saving of healthcare expenses.

Ileal interposition (IT) surgery involves the insertion of a segment of the ileum into the proximal intestine (jejunum), providing a surgical model whereby the endocrine effects of bariatric surgery on distal gastrointestinal hormone production can be isolated and mechanistically evaluated. In the early 2000s, IT surgery was shown to induce weight loss and improve insulin signaling in obese animal models (*i.e.*, Goto-Kakizaki and streptozotocin-treated rats), exhibiting a pathophysiology that is more similar to type-1 diabetes (4–6). Subsequently, we extended the knowledge in the field, presenting findings supporting the efficacy and mechanisms by which IT surgery delays the onset of diabetes in a T2DM rodent model [University of California, Davis (UCD)-T2DM rats] developed in the laboratory of Dr. Havel at the University of California, Davis (7). This rodent model combines adult-onset polygenic obesity and insulin resistance with defective β-cell function, resulting in a T2DM pathophysiology that more closely reproduces the T2DM paradigm clinically observed in humans than other existing rodent models. Compared with most other rodent models of T2DM, the UCD-T2DM rat model has intact leptin signaling and exhibits insulin resistance with inadequate β-cell compensation, resulting in marked hyperglycemia in both the fasting and nonfasting states (7). Previous studies evaluating the effects of IT surgery in UCD-T2DM rats indicated that this procedure delayed diabetes onset, improved pancreatic insulin secretion and content, increased glucagon-like protein-1 and peptide-YY secretion, and lowered circulating lipids and ectopic lipid deposition without biologically relevant effects on either energy intake or body weight (8).

Glucose homeostasis is achieved *via* the integration of physiologic processes occurring in multiple organs, including fat depots. In particular, the liver is the primary site of endogenous glucose production by gluconeogenesis during prolonged fasting, and dysregulation in this pathway is a common feature in patients with T2DM. Considering that gluconeogenesis is a highly energy-dependent process that relies almost solely on mitochondrial fatty acid β-oxidation (FAO), it is not surprising that insulin resistance in liver and muscle can arise from defects in this pathway, leading to accumulation of intracellular lipid or fatty acid metabolites that ultimately suppresses insulin-stimulated glucose transport and metabolism (9, 10). Consequently, elucidating the pathways by which IT surgery delays the onset of diabetes and how it integrates the response from liver and other organs would allow a better understanding of the early stages of T2DM.

In the present study, we investigated the effect of IT surgery on hepatic gene expression and mitochondrial outcomes in liver, kidney cortex, skeletal muscle, heart, epididymal and inguinal adipose depots, cerebellum, and hindbrain from 2-mo-old UCD-T2DM rats prior to the onset of T2DM after 1.5 and 4.5 mo following IT surgery.

MATERIALS AND METHODS

Chemicals and biochemicals

EDTA, EGTA, sodium succinate, mannitol, sucrose, and HEPES were all purchased from MilliporeSigma (Burlington, MA, USA). Tris-HCl, glycine, sodium chloride, and potassium chloride were purchased from Thermo Fisher Scientific (Waltham, MA, USA). Bovine serum albumin (fatty acid free) was obtained from MP Biomedicals (Santa Ana, CA, USA). All other reagents were of analytical or higher grade.

Animals

The UCD-T2DM rats used for this study have been previously described in detail in refs. 11 and 12. The UCD-T2DM rat model was created by crossing Sprague-Dawley rats with adult-onset obesity and insulin resistance (but without overt T2DM) with lean ZDF rats that were homozygous wild type for the leptin receptor gene but known to have a defect in insulin gene transcription and islet function (13). Male UCD-T2DM rats were individually housed on a 14–10 h light-dark cycle in wire cages in the animal facility of the Department of Nutrition at UCD. Nonfasting glucose levels were assessed weekly between 14:00–16:00 h with a glucose meter (One-Touch Ultra; LifeScan, Milpitas, CA, USA), with diabetes onset defined as testing a nonfasted blood glucose value >200 mg/dl (11.1 mM) for 2 consecutive weeks. At 2 mo of age, rats received IT surgery, sham surgery, or no surgery. Nonfasting blood glucose and circulating triacylglyceride (TAG) concentrations were followed in these groups for up to 4.5 mo after surgery. A separate cohort of rats from the IT ($n = 10$) and sham-treated ($n = 10$) groups were euthanized at 1.5 mo postsurgery for evaluating the hepatic transcriptome, mitochondrial parameters, and the lipid content in several tissues. An independent cohort of animals that did not undergo either sham treatment or IT surgical intervention [nondiabetic ($n = 4$) or diabetic ($n = 29$) UCD-T2DM rats] were used to assess mitochondrial outcomes in liver and inguinal fat. A subset of rats that did not receive sham or IT surgery ($n = 4$/group; nondiabetic and diabetic for 120–150 d) were used for the evaluation of ATP-driven oxygen uptake. All experimental protocols were approved by the UCD Institutional Animal Care and Use Committee, and followed National Institutes of Health (Bethesda, MD, USA) guidelines.

Surgery

The procedure for IT surgery was performed as previously described in refs. 11 and 14. Rats were fed a liquid diet (Boost; Novartis, Basel, Switzerland) 4 d before the surgical procedure and 7 d after the surgeries. A dose of enrofloxacin (20 mg/kg/d, s.c.) was administered prior to and after surgery. Anesthetic induction and maintenance were performed with isoflurane (1–5%). A midline abdominal incision was performed, and a segment of ileum (~10 cm) ~5–10 cm proximal to the ileocecal valve was transected. The ends of the ileum were anastomosed

using a 7-0 polydioxanone suture (Johnson & Johnson, New Brunswick, NJ, USA). The isolated ileal transection was then interposed 5–10 cm distal to the ligament of Treitz with its vasculature supply. Rats that underwent sham surgery were subjected to the same protocol; however, transections made in the identical location were anastomosed in their original position without translocation.

Tissue collection

At 1.5 mo after either IT sham surgery (at ~3.5 mo of age), rats were euthanatized with an overdose of pentobarbital (200 mg/kg i.p.), and the following tissues were harvested: liver, kidney cortex, skeletal muscle, heart, epididymal adipose depot, inguinal adipose depot, cerebellum, and hindbrain. The adipose depot collections were performed avoiding the collection of the corresponding adjacent lymph nodes and blood vessels. All tissues were washed with cold PBS, and mitochondria were isolated immediately as reported before in detail by Giulivi *et al.* (15) and as described briefly below.

Hepatic gene expression

Microarray analysis was carried out by standard procedures as described in the Agilent Technologies (Santa Clara, CA, USA) single-color expression array manual using RNA samples from 4 animals from each group 1.5 mo after sham or IT surgery that were subjected to microarray analysis. The procedures for microarray, data analysis, and gene expression validation are provided in detail as follows: RNA extraction: portions of liver tissue (up to 10 mg) were snap frozen for RNA extraction. Tissue was homogenized in 5 ml Trizol reagent (Thermo Fisher Scientific) followed by the addition of 1 ml of chloroform and centrifugation at 12,000 *g* for 15 min. The collected supernatants were purified with the RNeasy Mini Kit (Qiagen, Hilden, Germany). RNA quality was determined with an Agilent 2100 Bioanalyzer (Agilent Technologies), and the yield was evaluated with a Tecan M200 Infinite microplate reader (Tecan, Männedorf, Switzerland). Each sample was analyzed individually. Microarray and data analysis: 10 μg of RNA from each sample was used for probe labeling with the SuperScript indirect cDNA labeling system (Thermo Fisher Scientific). Probes were hybridized to SurePrint G3 Rat GE 8 × 60k Microarray (v.9.1; Agilent Technologies) following the manufacturer's instructions. These arrays contain 30,584 entrez gene RNAs. Feature Extraction v.9.1 software (Agilent Technologies) was used to filter, normalize, and calculate the signal intensities. Gene expression profiling analysis was conducted using Partek Genomics Suite (Partek, St. Louis, MO, USA). The probe intensity data were $\log_2$ transformed and then quartile normalized to make uniform the distribution of probe intensities for each array within the set of experiments. Low- or nonexpressed probes were filtered out if samples' intensity values fell below the predetermined $\log_2$-based value. The filtered intensity data were subjected to a Student's *t* test to generate *P* values and fold change values. This process generated a 3195–rat loci temporary gene symbol (LOC) list. By substituting the LOC nomenclature for official gene symbols by using the functional annotation tools of Database for Annotation, Visualization and Integrated Discovery (DAVID) [v.6.8 (16, 17)] and g:Profiler (18), 2807 remained after cleaning the list of genes that are no longer annotated or had insufficiently characterized LOC. Pathway enrichment analysis was performed with InnateDB [using a $\log_2$ fold change (FC) cutoff of 1; $P \leq 0.05$] and using the hypergeometric algorithm with the Benjamini-Hochberg correction method (19). To confirm the pathway enrichment analysis using a different algorithm and database, we used PathVisio (20) with the WikiPathway database (21). This last analysis was further filtered by setting a cutoff of ≥5 genes per pathway, *z* scores ≥2, and $P \leq 0.05$. To better visualize the pathway enrichment, Pathview Web was used (22). Validation of gene expression: quantitative RT-PCR (qRT-PCR) assays were performed with an Eppendorff Mastercycler using iScript one-step RT-PCR kit probes (Bio-Rad, Hercules, CA, USA). The primers and probe mix for the TaqMan gene expression assay for target genes [beta-2-microglobulin, glyceraldehyde 3-phosphate dehydrogenase (*GAPDH*), hypoxanthine phosphoribosyltransferase 1 (*HPRT1*), pyruvate dehydrogenase kinase 4 (*PDK4*), β-actin (*ACTB*), NADH dehydrogenase 1 (*ND4*), cytochrome B (*CYB*), pyruvate kinase (*PK*), NADH dehydrogenase 4 (*ND4*), and lipin (*LPIN*)] were from Roche (Basel, Switzerland). According to microarray results, expression of GAPDH was not significantly altered between samples; thus, GAPDH was used as the internal control. qRT-PCR reactions were carried out in a total volume of 20 μl. iScript Kit instructions were followed for the thermocycling steps. A standard curve using serially diluted samples was made for each experiment. Data were analyzed with the software provided by the manufacturer. The RNA levels of the target genes in the template were calculated from standard curves. The correlation between the microarray data and the expression of these genes obtained with qRT-PCR was 0.843 ($P = 0.0022$; Supplemental Fig. S1).

Mitochondrial outcomes

Mitochondrion-enriched tissue fractions were isolated as previously reported by Napoli *et al.* (23). Briefly, tissues (1–5 mg wet weight) were washed extensively with cold PBS (to remove blood) and centrifuged at 300 *g* for 10 min. Tissues were subsequently homogenized in 0.25 M sucrose, and the suspension was centrifuged at 1500 *g* for 10 min at 4°C to remove tissue debris. The supernatant was centrifuged at 10,000 *g* for 20 min to precipitate mitochondria. Mitochondria-enriched pellets were resuspended in 200 μl of 0.25 M sucrose and 2 mM EDTA containing kinase, phosphatase, and proteolytic inhibitors frozen immediately in liquid nitrogen and used for enzymatic analyses within 2 wk. Oxygen consumption was evaluated under phosphorylating and nonphosphorylating conditions, with NAD- and FAD-linked substrates (23) using a Clark-type oxygen electrode (HansaTech, Osterholz-Scharmbeck, Germany) as described by Napoli *et al.* (23). Mitochondrial samples (10–20 μg protein) were added to the oxygen chamber in a buffer containing 0.22 M sucrose, 50 mM KCl, 1 mM EDTA, 10 mM KH_2PO_4, and 10 mM HEPES at pH 7.4. The ATP-driven oxygen consumption rates were evaluated in the presence of 1 mM ADP and 1 mM malate-10 mM glutamate followed by the addition of 5 μM rotenone and 10 mM succinate followed by the addition of 3.6 μM antimycin A. Activities were tested after lysing mitochondrial-enriched fractions in 20 mM HEPES at pH 7.4 supplemented with proteolytic and phosphatase inhibitors (P2714 and P8849; MilliporeSigma). NADH-decylubiquinone oxidoreductase (NQR), succinate-cytochrome C reductase (SCCR), cytochrome *c* oxidase (CCO), and citrate synthase (CS) activities were evaluated by spectrophotometry as described before in detail in refs. (24 and 25) using an Infinite M200 plate reader (Tecan).

Statistics

Mitochondrial outcomes, circulating TAG levels. and tissue lipid content were analyzed with a 2-tailed Student's *t* test (between IT and sham surgery) with the level of significance

set at $P \leq 0.05$. Statistical analysis of the nonfasting glycemia and circulating TAG levels at different time points was performed with a 2-way ANOVA followed by Dunnett's or Sidak's multiple comparisons tests where indicated. The Mantel-Cox test was used for the analysis of diabetes incidence. All statistical tests were performed by using Prism software (v.7.03, GraphPad, La Jolla, CA, USA).

RESULTS

IT surgery delays the onset of type 2 diabetes as determined by nonfasting glycemia

Nonfasting glycemia (evaluated as indicated in the Materials and Methods) was monitored weekly for up to 4.5 mo postsurgery in a cohort of UCD-T2DM rats that were 2-mo old at the time of IT surgery, sham surgery, or neither surgery (nonsurgical controls). Diabetes onset was defined as a nonfasted blood glucose concentration >200 mg/dl (11.1 mM) for 2 consecutive weeks. Because no statistically significant differences were observed in glycemia ($P > 0.873$) or diabetes incidence ($P = 0.905$) between control and sham-treated groups at any time point, only IT- and sham-treated animals underwent further analysis.

Body weight was assessed 1 wk before surgery and up to 13 wk after IT (**Fig. 1*A***). No statistically significant differences in body weight were recorded between sham and IT surgeries (Fig. 1*A*). From week 13 onward following the surgeries, sham-treated rats showed statistically significant increases of nonfasting glycemia (Fig. 1*B*) whereas IT rats showed no statistically significant changes compared with presurgical glucose values. Ten of sixteen rats in the sham-treated group were diagnosed with diabetes during the 19-wk testing period [dotted line on Fig. 1*B*; nonfasting glycemia >200 mg/dl for 2 wk (11)] compared with only 5 rats of 16 rats that received IT surgery (Fig. 1*C*). Major contributors to the differences in nonfasting glucose levels between sham and IT surgery were time ($F = 28.35$; $P <$

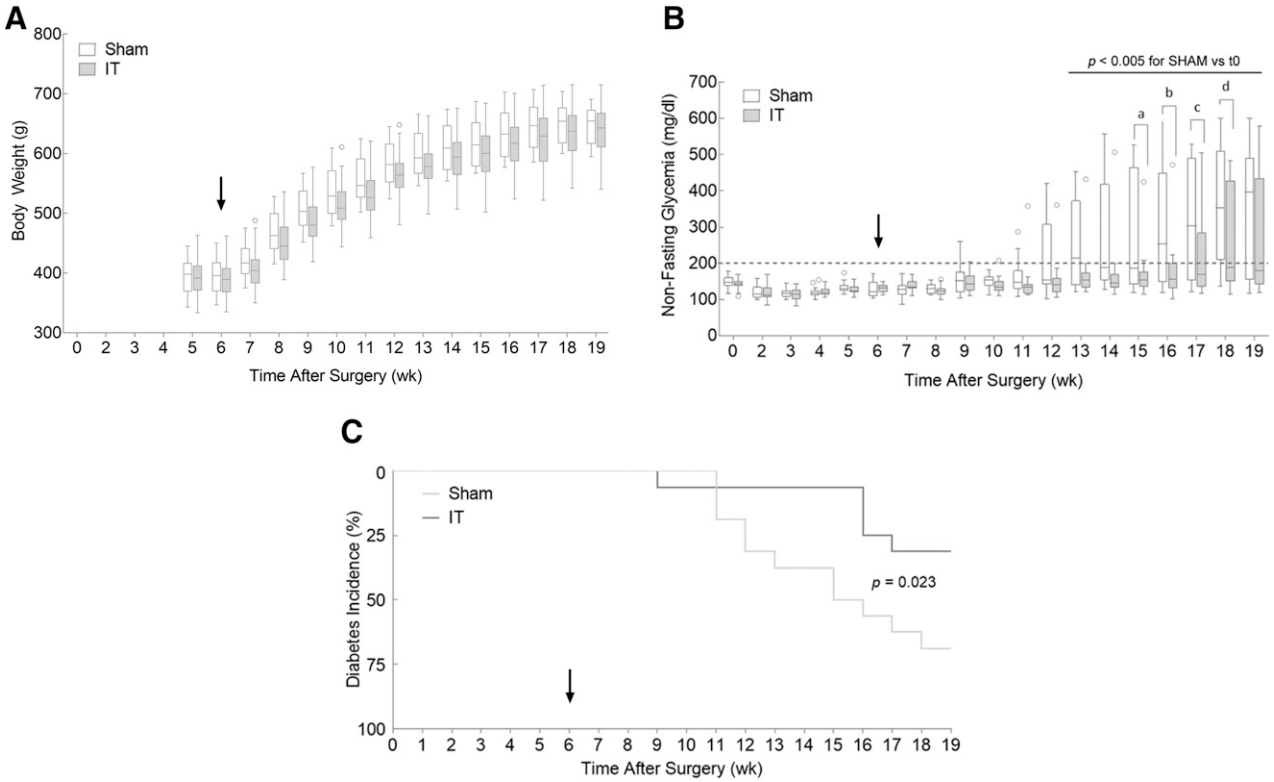

Figure 1. Development of diabetes in UCD-T2DM rats after sham and IT surgery. *A*) Body weight was assessed for 14 wk in sham-treated and IT animals. Statistical analysis was performed with 2-way ANOVA followed by Sidak's multiple comparisons *post hoc* test. Although both treatment and time accounted respectively for 0.63 and 84.5% of the overall body weight variance recorded in the 2 groups ($F = 26.37$, $P < 0.0001$ for treatment; $F = 253.5$, $P < 0.0001$ for time), no statistically significant differences were identified between the sham and IT surgery at any time point. *B*) Nonfasting blood glucose concentrations were followed for 4.5 mo in male 2-mo-old UCD-T2DM rats. Animals were randomly assigned to each of the 2 groups: sham treated ($n = 16$) or IT treated ($n = 16$). The arrow indicates the time at 1.5 mo after sham or IT surgery. Criteria for a diagnosis of diabetes were ≥200 mg/dl for 2 consecutive weeks (indicated with a dashed line). Data are shown as Tukey box plots to visualize outliers in each of the 2 groups tested (darker open circles for sham surgery and lighter open circles for IT surgery). Two-way repeated-measure ANOVA was used to evaluate the contributions of time ($F = 28.35$; $P < 0.0001$), treatment ($F = 4.53$; $P < 0.0001$), and their interaction ($F = 3.98$; $P = 0.0007$) on the nonfasting glucose levels. Sidak's multiple comparisons test was used to evaluate statistically significant differences between sham and IT surgery at each time point. *a*, $P = 0.0018$; *b*, $P = 0.0014$; *c*, $P = 0.0388$; *d*, $P = 0.0117$. Dunnet's multiple comparison test was used to evaluate statistically significant differences at each time point relative to time 0 in either sham or IT surgery. Week 13, $P = 0.0020$; wk 14, $P = 0.0006$; wk 15–19, $P = 0.0001$ for sham surgery with no significance for IT surgery. *C*) Incidence of rats with diabetes after sham or IT surgery. Statistical analysis was performed with the log-rank (Mantel-Cox) test.

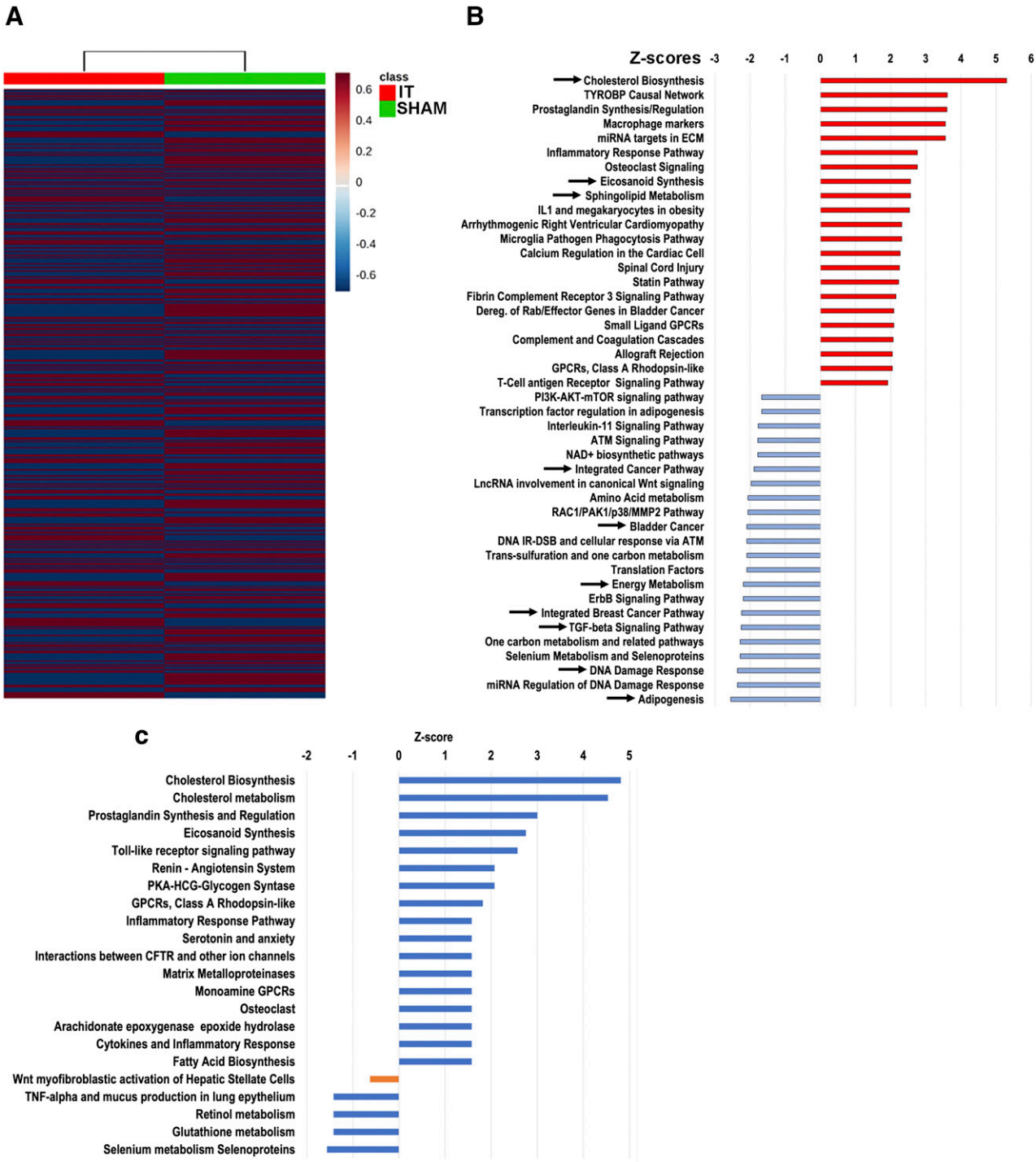

Figure 2. Hepatic signaling pathways affected by IT surgery. Hepatic gene expression in liver collected at 1.5 mo post-IT surgery *vs.* sham surgery. *A*) A total of 2807 genes were found to be differentially expressed, with the majority of them (2074) being down-regulated as partly shown in the heat map. The 28 pathways identified as statistically relevant are reported in Table 1. *B*) Enrichment analysis indicated the up-regulation of lipid pathways (cholesterol and eicosanoid syntheses and sphingolipid metabolism), whereas adipogenesis, energy metabolism, amino acid metabolism, and the PI3K-Akt-mTOR pathway were found to be down-regulated. *C*) Enrichment analysis was performed with the PathVisio tool using the species *Rattus norvegicus* in which the HSC activation pathway is included. This analysis confirmed the up- and down-regulation of pathways identified before using human databases but with the inclusion of HSCs (in orange). ATM, ataxia telangiectasia mutated; CFTR, cystic fibrosis transmembrane conductance regulator; ECM, extracellular matrix; ErbB2, receptor tyrosine kinase 2; HCG, human chorionic gonadotropin; IR-DSB, ionizing radiation-induced double strand breaks; lncRNA, long non-coding RNAs; miRNA, microRNA; MMP2, matrix metallopeptidase 2; PAK1, P21 (RAC1)-activated kinase 1; RAC1, Ras-related C3 botulinum toxin substrate 1; TYROBP, TYRO protein tyrosine kinase-binding protein.

0.0001) and the interaction between time and surgical intervention ($F = 3.98$; $P < 0.0001$), followed by surgical intervention alone ($F = 4.53$; $P = 0.042$) (Fig. 1*B*).

Diabetes incidence in the sham-treated group *vs.* post-IT was 2-fold greater ($P = 0.023$ by Mantel-Cox test; Fig. 1*C*). By using the Kaplan-Meier estimator (and using Fig. 1*C* input data), we calculated that 50% of the sham-treated rats would develop diabetes within 91 d (13 wk) whereas for those that received IT surgery, it would take ~185 d (~25 wk). Importantly, this 3-mo onset delay is not negligible as this onset delay would then translate to ~9 human years (1 adult rat month is comparable to 3 human years (26) and the caveat that both species may not develop diabetes at the exact same rate during the period tested). These results are similar to what we previously reported from an earlier study of the effects of IT surgery on diabetes onset in UCD-T2DM rats (8).

IT surgery impacts hepatic signaling pathways not traditionally associated with either insulin or glucagon signaling

To assess early changes mediated by IT surgery on bioenergetics, we studied male rats (2 mo of age at the time of surgery), 1.5 mo postsurgery because at this time point (Fig. 1 indicated with an arrow), none of the animals that underwent either IT or sham surgery had developed diabetes (11, 14). Hepatic gene expression obtained at 1.5 mo post-IT surgery *vs.* sham surgery indicated a total of 2807 genes were differentially expressed, with the majority of them being down-regulated (2074 or 74% of the total; **Fig. 2*A***). Pathway enrichment analysis (which summarizes the level of differential expression of genes in the pathway relative to a null distribution) in conjunction with a topology analysis [Metaboanalyst using the Kyoto Encyclopedia of Genes and Genomes (KEGG) database] indicated 28 pathways as statistically relevant (**Table 1**). Signaling by TGF-β was the most important pathway, followed by B-cell receptor and peroxisome proliferator-activated receptor (PPAR) signaling pathways (Table 1). Pathways associated with cancer (including thyroid, renal, leukemia, prostate, kidney, and lung; Fig. 2*A* and Table 1) suggested an involvement of pathways regulating cell proliferation and differentiation. Surprisingly, insulin signaling and maturity onset diabetes of the young, although still significant, had lower relevance than the others mentioned above (positions 10 and 16, respectively).

Enrichment analysis (set at a cutoff of ≥5 genes/pathway and $P \leq 0.05$; PathVisio with WikiPathway database; Fig. 2*B*) indicated the up-regulation of lipid metabolism pathways (cholesterol and eicosanoid syntheses, sphingolipid metabolism; Fig. 2*B*), consistent with the enrichment and topology observed for steroid biosynthesis (Fig. 2*B* and Table 1) and with the previously reported higher levels of circulating bile acids in IT- *vs.* sham-treated rats (14). Similarly, the extracellular matrix organization was also up-regulated. Conversely, the most down-regulated pathways were adipogenesis, DNA damage response, TGF-β signaling, energy metabolism, and those underlying several types of cancer (Fig. 2*B*).

TABLE 1. *Hepatic pathway enrichment analysis in IT rats*

Pathway	Total	Hits	*P*
TGF-β signaling pathway*	84	26	0.0003
B-cell receptor signaling pathway	75	22	0.0021
PPAR signaling pathway	64	19	0.0035
Valine, leucine, and isoleucine degradation	44	14	0.0059
FcRγ-mediated phagocytosis	97	25	0.0072
Chronic myeloid leukemia	73	20	0.0076
Thyroid cancer	28	10	0.0079
Renal cell carcinoma	60	17	0.0094
Nonsmall cell lung cancer	52	15	0.0120
Insulin signaling pathway	137	32	0.0121
Viral myocarditis	26	9	0.0144
Nicotinate and nicotinamide metabolism	26	9	0.0144
Steroid biosynthesis	18	7	0.0154
Pyruvate metabolism	41	12	0.0210
Pathways in cancer	310	62	0.0239
Maturity onset diabetes of the young	24	8	0.0261
Glycine, serine, and threonine metabolism	33	10	0.0266
ErbB signaling pathway	87	21	0.0269
Prostate cancer	87	21	0.0269
Selenocompound metabolism	12	5	0.0292
Bile secretion	29	9	0.0299
Vascular smooth muscle contraction	109	25	0.0306
Inositol phosphate metabolism	58	15	0.0321
Cysteine and methionine metabolism	34	10	0.0326
Butanoate metabolism	25	8	0.0333
Synthesis and degradation of ketone bodies	9	4	0.0401
mTOR signaling pathway	45	12	0.0420
VEGF signaling pathway	76	18	0.0458

Detailed results from the pathway analysis. Total represents the total number of proteins in the pathway. Hits represents the matched number from the uploaded data. Original *P* value was calculated from the enrichment analysis. *$P < 0.01$ ($P = 0.0737$; Holm-Bonferroni adjusted). ErbB, receptor tyrosine kinase 2.

The combined pathway analysis (Fig. 2 and Table 1) indicated that the down-regulation of the TFG-β signaling pathway (Supplemental Fig. S2) was a central feature of IT surgery, highlighting the fact that the impact of IT surgery on type 2 diabetes was not solely linked to those traditionally associated to improvements in insulin signaling (Supplemental Fig. S3), PI3K-Akt–mechanistic target of rapamycin (mTOR) (Supplemental Fig. S4), PPAR (Supplemental Fig. S5), or adipocytokine pathways (Supplemental Fig. S6).

In terms of cellular composition, although the hepatic gene expression profile was consistent with the presence of hepatocytes, it also pointed at other nonparenchymal cells such as immune (B-cell receptor pathway; Table 1) and biliary epithelial cells (bile acid synthesis and secretion, Table 1). In this regard, the identification of TGF-β (Table 1 and Supplemental Fig. S2) and PPAR pathways (Table 1 and Supplemental Fig. S5), along with their involvement in hepatic stellate cell (HSC) activation [*i.e.*, process that involves the transition of lipid-storing pericytes to myofibroblastic cells favoring liver fibrosis and insulin resistance (27)] prompted us to rerun the pathway analysis. Because

HSC activation is not included in any of the *Homo sapiens*' pathway databases (Reactome, KEGG, WikiPathway), the differential expression of genes related to the differentiation/activation of HSC was performed with PathVisio using the WikiPathway database with the *Rattus norvegicus* species which includes this pathway. This analysis confirmed the up- and down-regulation of pathways identified before using the human databases (compare Fig. 2*B vs.* Fig. 2*C*) with the inclusion of the down-regulation of HSC activation (marked in orange; Fig. 2*C*). Consistent with reports indicating that PPARγ is required for the maintenance of differentiated HSC (**Fig. 3*A***) in a process analogous to that observed for the differentiation of adipocytes (28–30), a down-regulation of the adipogenic pathway was also observed (Figs. 2*B* and 3*B* and Table 1).

IT surgery impacts cholesterol and sterol syntheses and attenuates oxidative phosphorylation in key target gluconeogenic and glyceroneogenic tissues

In terms of metabolic pathways impacted by IT surgery, 2 were primarily up-regulated: steroid biosynthesis (including cholesterol, steroid, sterols, and bile acid

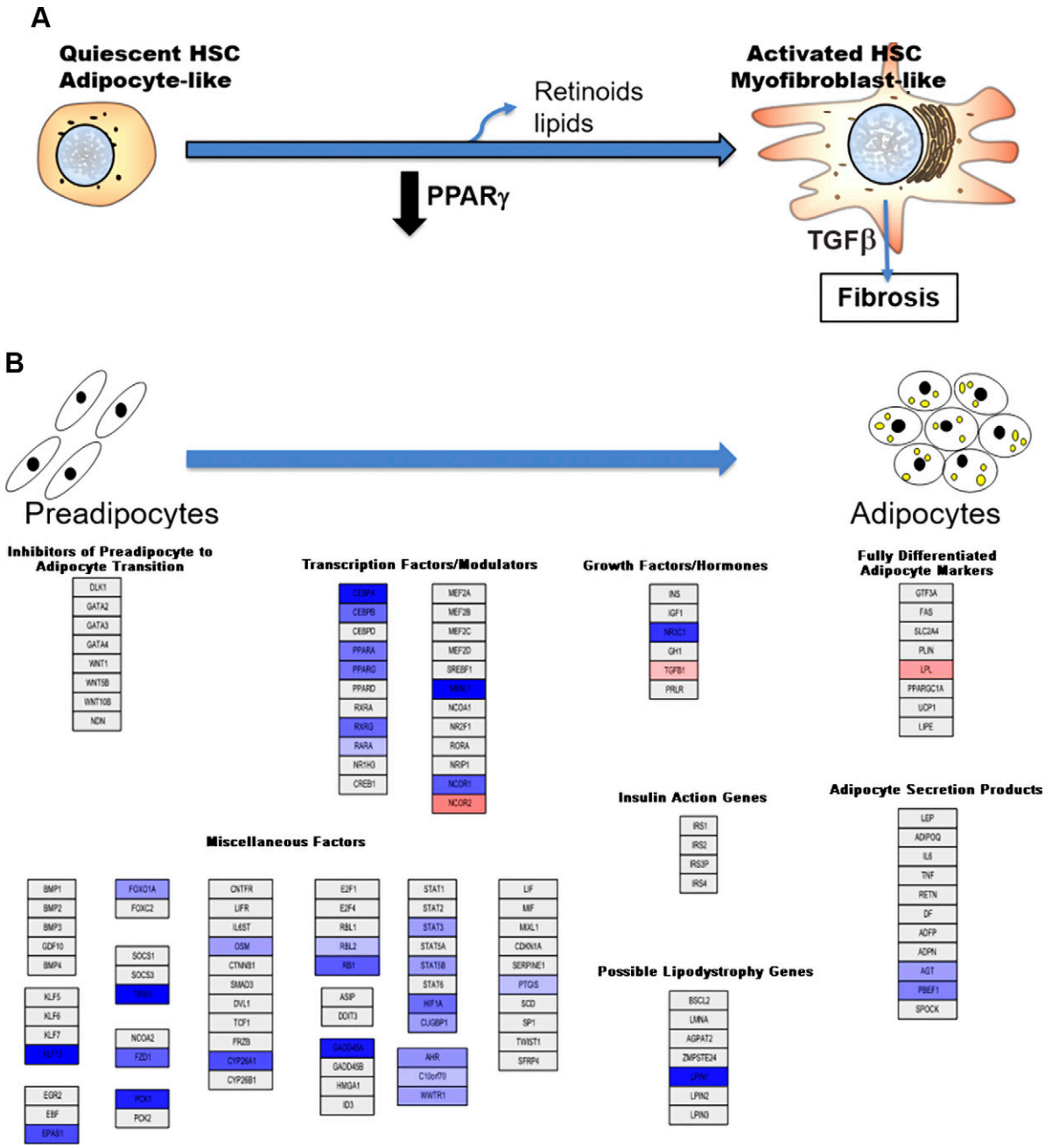

Figure 3. HSC activation–related gene expression levels and roles in adipogenesis. *A*) Scheme showing activation of HSCs and their role in hepatic fibrosis. Upon activation, HSCs transition to myofibroblasts, leading to fibrogenesis. A number of effectors can induce activation of HSCs, including paracrine signaling from damaged epithelial cells, scar tissue, immune impairment, and enteric dysbiosis. *B*) IT-dependent regulation (blue, down-regulated; red, up-regulated) of genes involved in adipogenesis.

metabolism and biosynthesis; Supplemental Fig. S7) and extracellular matrix organization (Fig. 2C and Table 1 and Supplemental Fig. S8).

Among the down-regulated metabolic pathways, fatty acid catabolism (β-oxidation; Supplemental Fig. S9), gluconeogenesis decreased gene expression of 2 key gluconeogenic enzymes: glucose-6-phosphatase (Log_2 FC = −0.70) and the rate-limiting step enzyme phosphoenolpyruvate carboxykinase (Log_2 FC = −0.85); (Supplemental Fig. S10) and bile secretion (Supplemental Fig. S11) as well as that of forkhead box (Fox) a2, which is required for activation of gluconeogenesis during fasting. Furthermore, insulin-regulated genes such as tyrosine aminotransferase and IGF binding protein 1, Foxo1a, and

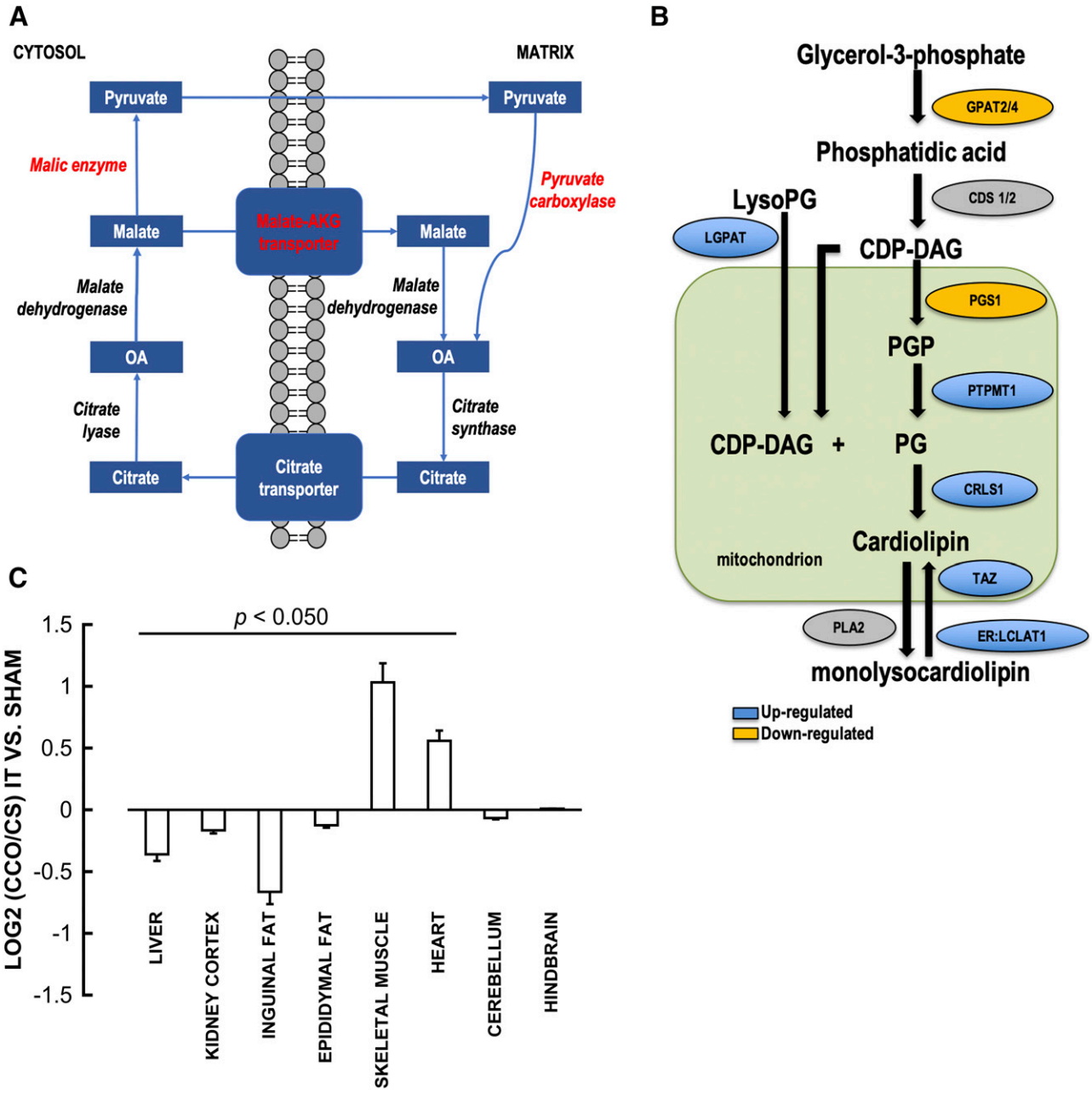

Figure 4. Impact of IT on mitochondrion-related gene expression and on selected mitochondrial outcomes in tissues collected from UCD-T2DM rats at 1.5 mo-post surgery. *A*) Fatty acid synthesis was down-regulated in response to IT surgery. Decreased gene expression of malic enzyme, pyruvate carboxylase, and the malate-oxoglutarate transporter is shown as red font. *B*) The lower synthesis of CL post-IT surgery is supported by the lower gene expression of key components of CL biosynthesis: CRLS1, lysocardiolipin acyltransferase (LCLAT1), CDP-diacylglycerol-3-phosphate 3-phosphatidyl transferase (PGS1), phosphatidylglycerophosphatase and protein-tyrosine phosphatase (PTPMT1), and tafazzin (TAZ). *C*) The activities of CS and complex IV (CCO) were evaluated in the indicated tissues at 1.5 mo post-IT (n = 10) or sham surgery (n = 10). Experimental details are presented in the Materials and Methods section. Activities were expressed as mU/mg [nmol product × (min × mg protein)$^{-1}$] and they are shown as natural log of the fold-change relative to sham surgery. Statistical analysis was performed using the 2-tailed Student's t test.

activating transcription factor 4 (the 2 latter genes act synergistically to trigger glucose intolerance and insulin insensitivity) were all down-regulated after IT surgery. Downstream targets of Foxo1a growth arrest and DNA damage inducible α and γ were also down-regulated in IT *vs.* sham surgery.

To assess the potential role of decreased gluconeogenesis and mitochondrial FAO to contribute to the IT-dependent delayed TD2M onset, we compared indices of mitochondrial function in tissues from IT- and sham-treated UCD-T2DM rats. To this end, we enriched the differentially expressed genes by filtering the data with the keyword "mitochondrion" as defined by the gene ontology cellular compartment to enrich for mitochondrial pathways that were affected by the IT surgery.

Based on the differentially expressed genes that encoded for mitochondrial proteins (n = 118), most of them were down-regulated (84%), and among them, the most down-regulated were fatty acid synthesis [with decreased gene expression of malic enzyme, pyruvate carboxylase, and the malate-oxoglutarate transporter (**Fig. 4*A***)] and glycerolipid metabolism with a clear impact on cardiolipin (CL) synthesis (Fig. 4*B*, Supplemental Fig. *S*12). The lower synthesis of CL post-IT surgery is supported by the lower gene expression of key components of CL biosynthesis, including CL synthase 1 (CRLS1), the last step in CL biosynthesis, lysocardiolipin acyltransferase, cytidine diphosphate (CDP)-diacylglycerol-3-phosphate 3-phosphatidyl transferase, phosphatidylglycerophosphatase and protein-tyrosine phosphatase, and tafazzin (Fig. 4*B*).

Notably, CL is a mitochondrion-specific phospholipid that stabilizes the assembly of respiratory chain complexes, allowing full-yield oxidative phosphorylation (oxphos) output (31), especially in terms of the terminal oxidase of the electron transport chain complex IV or CCO (31). This activity was normalized to that of CS because it is a stable matrix mitochondrial enzyme whose activity is not generally subjected to fluctuations or pathologic changes, and it can be used as a surrogate marker for mitochondrial matrix mass (24, 32). The normalized activity of CCO was assessed in several tissues collected at 1.5 mo after surgery (selected based on both availability and their response to insulin as well as others not usually studied in T2DM such as cerebellum and hindbrain; Fig. 4*C*). None of the other mitochondrial complex activities evaluated (namely, complex I and complex II-III) were different between groups (Supplemental Fig. S13), suggesting a specific effect of IT surgery on CCO activity. Similarly, no differences were observed at 4.5 mo postsurgery (Supplemental Fig. S13) in any of the enzymatic activities tested (including CCO). This indicated that IT surgery is likely to have a relatively short-term effect (14) as we previously reported for endoplasmic reticulum stress response mitigation and adipose tissue remodeling after IT surgery (11).

These experiments were put into context by evaluating the tissue bioenergetics' status in liver and inguinal fat, 2 key insulin target tissues, at early stages of T2DM and at later periods when the diabetes had been established for >120 d. For the bioenergetics assessment, we focused on the complex I:complex II-III activity ratio as a surrogate marker for the mitochondrial use of available fuel (33, 34). This ratio is expected to increase when the oxidation of carbohydrates is more pronounced than that of fat and decreased when FAO is more prominent (*i.e.*, ratio of NADH:$FADH_2$ for glucose and, for instance, stearic acid, is 5:1 and 2:1, respectively, unless the reducing equivalents of glucose are imported by the less-common glycerol 3-phosphate shuttle). The complex I:complex II-III ratio decreased with T2DM progression in both tissues up to 2 mo postdiagnosis of diabetes, an opposite trend to that of CCO activity normalized to CS (**Fig. 5**). The decreased complex I:complex II-III ratios were consistent with increases in

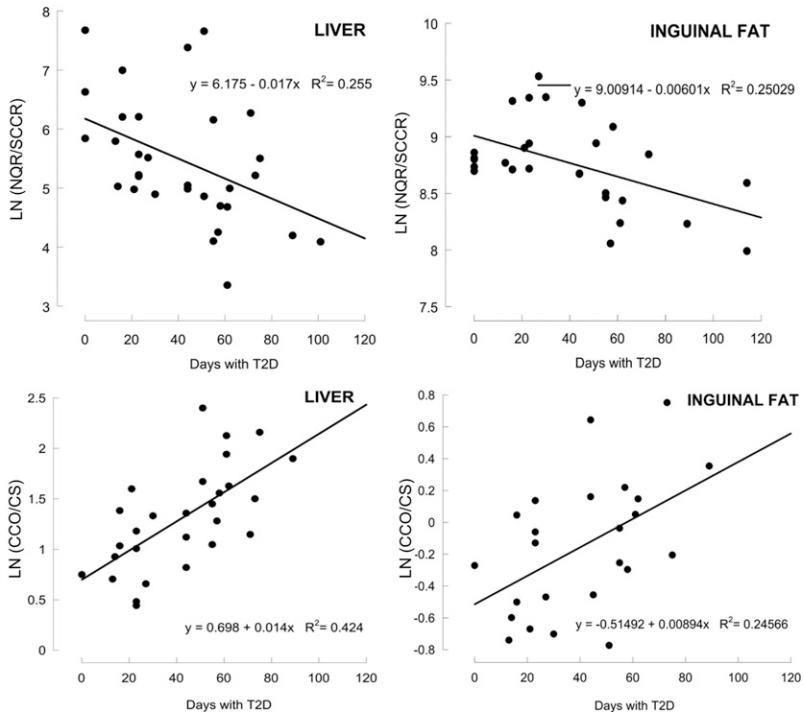

Figure 5. Changes in mitochondrial outcomes with T2DM progression in tissues from UCD-T2DM rats. Based on the abnormal nonfasting blood glucose (≥200 mg/dl for 2 consecutive weeks), rats were classified either as diabetic or nondiabetic (time 0). Those with diabetes (n = 29) were euthanized at different time points following the onset of T2DM. Complex I (as judged by the NQR activity) and complex II-III (as judged by the SCCR) activity were evaluated in liver and inguinal fat (top panels), whereas bottom panels show the activity ratios of CCO:CS from each diabetic rat whenever both tissues were available and the amount of tissue was enough to test each activity in triplicates. Activities of complex I and complex II-III were evaluated at the same time point (Supplemental Fig. S12). Activities of complex I, II-III, and IV and CS at 4.5 mo postsurgery are shown in Supplemental Fig. S12. LN, natural log.

high energy–consuming processes such as hepatic gluconeogenesis and adipose glyceroneogenesis at early stages of T2DM. The increased CCO:CS ratio was interpreted as increased cristae density as an adaptive response (more prominent in liver) to accommodate the extra flux of NADH and $FADH_2$ arising from mitochondrial FAO.

Although both liver and inguinal adipose tissues exhibited the same trends with regard to changes in mitochondrial outcomes with the progression of T2DM (Fig. 5), the time required for a 50% change in the activity ratios for each tissue was significantly different (mean for both NQR:SCCR and CCO:CS: 46 ± 4 and 97 ± 19 d for liver and inguinal adipose depot, respectively). These results suggested that the changes associated with intermediary metabolism were affected (2-fold) faster in liver than in the inguinal adipose depot, indicating the critical role of liver in the metabolic reprogramming compared with that of inguinal adipose depot during the development of T2DM.

When T2DM had been established for a longer period (>4 mo), mitochondrial bioenergetics was severely hampered when compared with that at earlier stages of T2DM. Upon comparison of several segments of the electron transport chain from phosphorylating mitochondria from liver, skeletal muscle, and heart from rats that had T2DM for 120–150 d *vs.* prediabetic rats (**Fig. 6**), a consistent decline in the capacity to generate ATP in liver and skeletal muscle was observed regardless of the substrates tested.

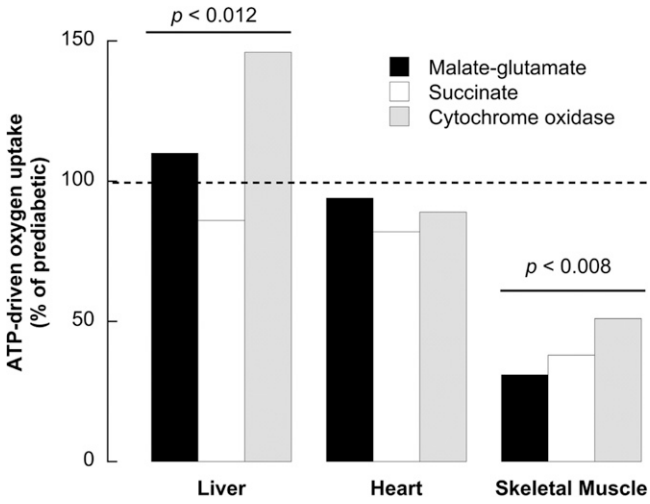

Figure 6. ATP-driven oxygen uptake by mitochondria from liver, skeletal muscle, and heart from T2DM-affected rats *vs.* prediabetic rats. Polarographic studies evaluated oxygen consumption by isolated mitochondria from liver, skeletal muscle, and heart from 4 male 3-mo-old nondiabetic UCD-T2DM rats and 4 male UCD-T2DM rats with diabetes for 120–150 d. This analysis was performed using a Clark-type oxygen electrode in the presence of various mitochondrial substrates and inhibitors to evaluate different segments of the electron transport chain [*e.g.*, malate-glutamate to donate NADH, succinate to donate $FADH_2$, and *N,N,N',N'*-tetramethyl-*p*-phenylenediamine (TMPD) plus ascorbate to donate electrons directly to cytochrome *c* to evaluate complex IV activity]. Data are shown as the mean of the percentage of that activity normalized to the mean of the prediabetic state. Statistics were performed by using the 2-tailed Student's *t* test.

This decline was not associated with changes of either coupling (between electron transport and ATP production) or oxygen uptake rate under nonphosphorylating conditions (state 4). The higher CCO activity in liver (in the absence of any other change) could be interpreted as an attempt to increase mitochondrial mass or ATP output to overcome cellular energy shortage.

DISCUSSION

In previous studies (7, 8, 14), we reported mechanisms potentially involved in the beneficial metabolic effects of IT surgery. These included increased circulating bile (cholic) acid levels, which we postulated to explain the decreased endoplasmic reticulum stress and inflammation; the improvement of insulin signaling in adipose, liver, skeletal muscle and pancreas; and the enhanced glucose-stimulated insulin secretion and preservation of islet integrity and β-cell mass following IT surgery (8, 14, 35). Recently, we reported that IT surgery had a more profound and prolonged effect on mesenteric fat depot than the other adipose depots that were studied (inguinal, epididymal, or retroperitoneal) (11). This specific effect on mesenteric adipose tissue was associated with changes that would be expected to ensue in a delay in the maturation of adipocytes (11).

In this study, we examined hepatic gene expression as well as mitochondrial outcomes of several tissues in UCD-T2DM rats following IT or sham surgery at 1.5 mo, a time when none of the animals had yet developed diabetes, to elucidate the mechanisms underlying the effects of IT surgery on the management of high energy–requiring processes such as gluconeogenesis and glyceroneogenesis. In response to insulin resistance, gluconeogenesis in liver is enhanced to improve the perceived hypoglycemia. The beneficial effect of IT surgery was exerted by the combined effect on the suppression of gluconeogenesis with an improved insulin-to-glucagon response based on the enrichment of the PI3K-Akt, insulin, adipokine, and PPARγ signaling pathways reinforced by the changes in the transcriptome in response to IT surgery. However, to our surprise, the combined pathway analysis (Fig. 2 and Table 1) revealed that the TFG-β pathway was substantially affected (down-regulated) by IT compared with sham surgery, suggesting that IT surgery was not solely linked to those pathways traditionally associated with delayed T2DM such as PI3K-Akt-mTOR PPAR, insulin, and adipocytokine pathways. In regard to the last pathway, biologic responses by adiponectin (a major adipocytokine) are mediated by binding with its receptors, adiponectin receptor (AdipoR) 1 and AdipoR2. Whereas AdipoR1 is abundantly expressed in skeletal muscle and in activated HSCs, AdipoR2 is predominantly expressed in other types of liver cells (36), with macrophages expressing both AdipoR1 and AdipoR2 (37). Relevant to our data, the overexpression of AdipoR2 (ADIPOR; Supplemental Fig. S6) and the ensuing signaling activation could be interpreted as an attempt at modulating oxidative stress and inflammation in liver (38). This is based on a report indicating that this receptor contributes to the

suppression of TGF-β–induced reactive oxygen species production in hepatocytes *via* enhancing PPARα activity and expression of catalase (39), thereby preventing the progression of nonalcoholic steatohepatitis to the stage of fibrosis. However, in our model, the overexpression of Adipor2 was not associated with the overexpression of its downstream targets (Supplemental Fig. S6), suggesting overall decreased adipokine signaling.

Several examples from the literature are consistent with a critical role for TFG-β signaling in T2DM. Liver-specific mothers against decapentaplegic homolog 3 (Smad3) and TGF-β1 receptor I–conditional knockout mice showed improved glucose tolerance with suppression of gluconeogenesis and enhanced insulin sensitivity, likely *via* the targeting of protein phosphatase 2–AMPK-FOXO1 by TGF-β1/Smad3 (40). Newly diagnosed patients with T2DM show lower levels of circulating TGF-β1 (41), whereas higher levels are associated with subjects with established T2DM (41, 42), and some antidiabetic treatments (including metformin) effectively reduced circulating TGF-β1 concentrations in subjects with T2DM (43). It is possible that IT-mediated down-regulation of both the PPARγ and TGF-β1 pathways suppressed the activation of HSCs and an overall lower hepatic oxphos to sustain gluconeogenesis, which contributes to hyperglycemia. In support of this mechanism, the TGF-β pathway is linked to PPARγ signaling in the activation of HSCs. HSCs normally reside in the space of Disse in a quiescent, nonproliferative state. They are characterized by abundant lipid droplets composed of retinyl esters, triglycerides, cholesteryl esters, cholesterol, phospholipids, and free fatty acids (44). During hepatic injury, quiescent HSCs undergo profound phenotypic changes, including enhanced cell proliferation, loss of lipid droplets, and excessive production of the extracellular matrix in a process named activation (30). As such, they are considered key players in the development of hepatic fibrosis, regardless of etiology (45–47). The transdifferentiation process requires decreased PPARγ signaling and activated HSC release or targeting by TGF-β1 to promote proliferation, extracellular matrix expression, hepatocyte apoptosis, and liver fibrosis (27). Because none of the rats at 1.5 mo post-IT showed either hyperglycemia or activation of hepatic gluconeogenesis, the main involvement and down-regulation of the TGF-β pathway provided an additional mechanism by which IT surgery might be playing a role at delaying the onset of T2DM by decreasing TGF-β1 a proinflammatory cytokine known to be 1 of the major activators of HSCs (46).

The up-regulation of cholesterol and bile syntheses in IT surgery deserves a separate discussion that takes into account not only TFG-β signaling but also the fate of bile acids in this surgical intervention. It is known that up-regulation of TGF-β1 signaling activates cholesterol 7α-hydroxylase (CYP7A1) expression, a gene whose product is directly involved in the biosynthesis of bile acids catalyzing the first and rate-limiting steps in the neutral or classic bile acid biosynthetic pathway. In turn, bile acids may activate intestinal Farnesoid X receptor to induce fibroblast growth factors 15–19, which are transported to the liver to stimulate liver regeneration (34) and inhibit further CYP7A1. However, in our model, CYP7A1 (despite the down-regulation of TGF-β) appeared as 1 of the most up-regulated genes. This apparent discrepancy can be bridged considering that CYP7A1 is regulated by a negative-feedback repression loop with its own biosynthesis at the level of gene transcription (48, 49). Therefore, the up-regulation of cholesterol and bile acid biosynthesis following IT surgery may be an attempt to meet the higher demands of the bile acid pool, which is depleted by bile acid diversion because IT surgery delivers incompletely digested nutrients as well as biliary and pancreatic secretions to the distal intestine and could be partially responsible for the delayed onset of T2DM.

It has been proposed that insulin resistance in liver and muscle can arise from defects in mitochondrial FAO, leading to accumulation of intracellular lipid and fatty acid metabolites that ultimately suppresse insulin-stimulated

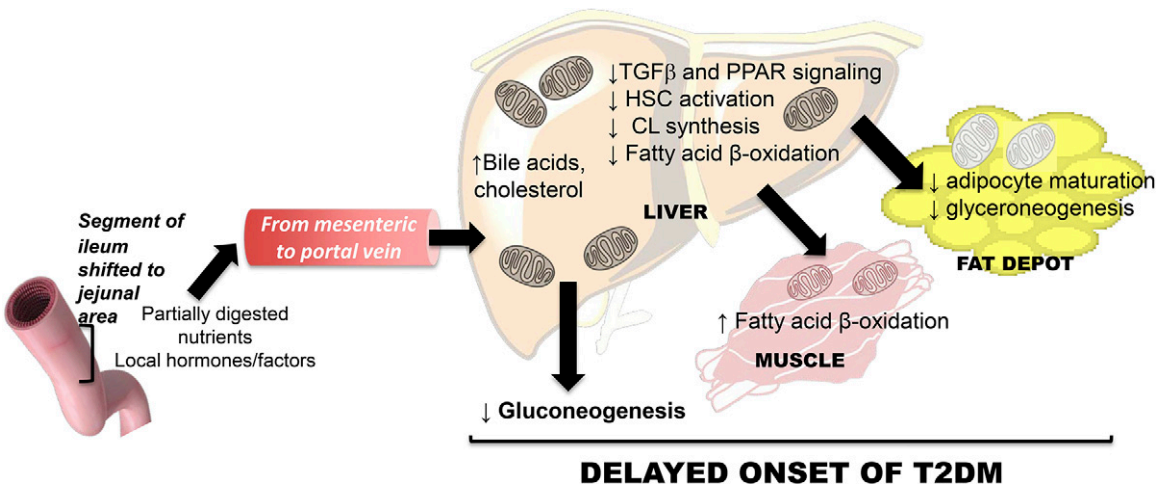

Figure 7. Mechanism underlying the IT-mediated delayed onset of T2DM. Undigested food passing through the intestine may trigger the release of chemokines, which reach the liver *via* portal circulation, thereby attenuating TGF-β1 signaling. The resulting increased hepatic bile acid levels and cholesterol biosynthesis as well as lowered CL biosynthesis may hamper mitochondrial FAO to sustain high-energy processes such as gluconeogenesis and glyceroneogenesis.

glucose transport and metabolism (9, 10). However, decreased oxphos has demonstrated beneficial effects in diabetes because it enhances insulin sensitivity (as assessed by increased Akt phosphorylation) (50), and metformin [an inhibitor of complex I among other targets (51)] has strong anti-inflammatory and antioxidant activities (52) that also improve hepatic steatosis (53). The increased oxphos observed at early stages of T2DM seem to be prompted by the need to sustain high-energy processes. When T2DM is advanced, the lower oxphos capacity and the altered mitochondrial complex ratios are highly indicative of mitochondrial dysfunction (**Fig. 7**). Therefore, as the result of IT surgery, lower oxphos capacity in liver, kidney cortex, and fat depots would effectively limit high energy–demanding processes such as gluconeogenesis and glyceroneogenesis, delaying the onset of T2DM. This switch represents a potential remodeling of mitochondria to accommodate anabolic reactions in order to provide a steady supply of intermediates for the synthesis of cholesterol (acetyl–coenzyme A *via* citrate export) as well as heme (as a component of cytochromes, some of which are present in the cholesterol pathway). CCO-CS was lower in IT *vs.* sham surgery in liver, kidney cortex, and the 2 fat depots tested (Fig. 4*C*), tissues with relatively higher energy demand to sustain gluconeogenesis and glyceroneogenesis. Conversely, heart and skeletal muscle exhibited higher CCO-CS, favoring mitochondrial FAO. Because no other mitochondrial complex activities tested were different between groups, the effect of IT surgery seems to be specific to CCO activity. It is tempting to link the lower oxphos to the lower CCO activity (not observed with the other complexes tested) resulting from down-regulation of the CL pathway. The relevance of CL in mitochondria is evidenced by its relatively high concentration in mitochondrial inner membranes [~15% of total phospholipids (54, 55)], and the interdependence between CL biosynthesis and oxphos is illustrated by the activation of CRLS1 by the increases in matrix pH that accompany mitochondrial ATP production (56) and the up-regulation of CL synthesis (57) mediated by CL-dependent supercomplex formation and CCO activity (58).

In summary, incompletely digested nutrients transiting the gastrointestinal tract may trigger the release of some chemokines from this tissue, which upon arrival to the liver *via* the portal circulation lead to an attenuation of TGF-β1 signaling, resulting in increased hepatic bile acid and cholesterol biosynthesis and likely lower CL biosynthesis, preventing mitochondrial FAO to sustain high-energy processes such as gluconeogenesis and glyceroneogenesis (Fig. 7). Although some of these effects of IT surgery appear to be transient, it is important to understand that significantly delaying the onset of T2DM, even transiently, is beneficial considering the serious complications of diabetes and the inherent overall healthcare costs associated with the management of T2DM. The mitochondrial outcomes evaluated here may also be better predictors of T2DM than nonfasting glucose concentrations, with the potential advantage of being assessed in readily available tissues such as circulating peripheral monocytes or platelets. Indeed, lymphocytes have been shown to be useful sources of surrogate biomarkers for investigating the influence of metabolic changes when monitoring human populations (59, 60).

Further studies could provide additional insights regarding novel target alternatives (*e.g.*, inhibitors of TGF-β signaling) that may complement IT surgery to maximize its effects or similarly effective but longer lasting and less invasive procedures representing a better therapeutic option for patients. FJ

ACKNOWLEDGMENTS

The authors thank Dr. Bethany Cummings (University of California Davis; current affiliation: Cornell University College of Veterinary Medicine, Ithaca, NY, USA) for her skillful performance of all surgeries, and Sarah Wong (University of California Davis) for running all gene expression experiments. This study was funded by U.S. National Institutes of Health, National Institute of Diabetes and Digestive and Kidney Diseases Grant RC1 DK087307 (to P.J.H. and C.G.), and microarray studies were funded by a pilot grant from the Genome Core Center at the University of California, Davis (to C.G.). The authors declare no conflicts of interest.

AUTHOR CONTRIBUTIONS

P. J. Havel and C. Giulivi designed and obtained funding for the study; C. Hung and C. Ross-Inta prepared all biological samples and evaluated mitochondrial outcomes; A. L. Flores-Torres contributed to the microarray analyses and drafting of the manuscript; E. Napoli performed most of the statistical analyses and contributed to the writing of the manuscript and assembling of figures; J. Graham collected and processed data presented in Fig. 1; P. Froment and K. L. Stanhope revised and edited the manuscript; P. J. Havel provided the tissues used in this study and edited the manuscript; and C. Giulivi conceptualized the study, designed the experiments, analyzed the data, and wrote the initial draft of the manuscript.

REFERENCES

1. Centers for Disease Control and Prevention. (2017) *National Diabetes Statistics Report, 2017*, Centers for Disease Control and Prevention, US Department of Health and Human Services, Atlanta, GA
2. Fox, C. S. (2010) Cardiovascular disease risk factors, type 2 diabetes mellitus, and the Framingham Heart study. *Trends Cardiovasc. Med.* **20**, 90–95
3. Kannel, W. B., and McGee, D. L. (1979) Diabetes and glucose tolerance as risk factors for cardiovascular disease: the Framingham study. *Diabetes Care* **2**, 120–126
4. Patriti, A., Aisa, M. C., Annetti, C., Sidoni, A., Galli, F., Ferri, I., Gullà, N., and Donini, A. (2007) How the hindgut can cure type 2 diabetes. Ileal transposition improves glucose metabolism and beta-cell function in Goto-kakizaki rats through an enhanced Proglucagon gene expression and L-cell number. *Surgery* **142**, 74–85
5. Patriti, A., Facchiano, E., Annetti, C., Aisa, M. C., Galli, F., Fanelli, C., and Donini, A. (2005) Early improvement of glucose tolerance after ileal transposition in a non-obese type 2 diabetes rat model. *Obes. Surg.* **15**, 1258–1264
6. Strader, A. D., Clausen, T. R., Goodin, S. Z., and Wendt, D. (2009) Ileal interposition improves glucose tolerance in low dose streptozotocin-treated diabetic and euglycemic rats. *Obes. Surg.* **19**, 96–104

7. Cummings, B. P., Digitale, E. K., Stanhope, K. L., Graham, J. L., Baskin, D. G., Reed, B. J., Sweet, I. R., Griffen, S. C., and Havel, P. J. (2008) Development and characterization of a novel rat model of type 2 diabetes mellitus: the UC Davis type 2 diabetes mellitus UCD-T2DM rat. *Am. J. Physiol. Regul. Integr. Comp. Physiol.* **295**, R1782–R1793
8. Cummings, B. P., Strader, A. D., Stanhope, K. L., Graham, J. L., Lee, J., Raybould, H. E., Baskin, D. G., and Havel, P. J. (2010) Ileal interposition surgery improves glucose and lipid metabolism and delays diabetes onset in the UCD-T2DM rat. *Gastroenterology* **138**, 2437–2446, 2446.e1
9. Lowell, B. B., and Shulman, G. I. (2005) Mitochondrial dysfunction and type 2 diabetes. *Science* **307**, 384–387
10. Szendroedi, J., Phielix, E., and Roden, M. (2011) The role of mitochondria in insulin resistance and type 2 diabetes mellitus. *Nat. Rev. Endocrinol.* **8**, 92–103
11. Hung, C., Bronec, C., Napoli, E., Graham, J., Stanhope, K. L., Marsilio, I., Giron, M. C., Havel, P. J., and Giulivi, C. (2018) Adipose depot-specific effects of ileal interposition surgery in UCD-T2D rats: unexpected implications for obesity and diabetes. *Biochem. J.* **475**, 649–662
12. Kleinert, M., Clemmensen, C., Hofmann, S. M., Moore, M. C., Renner, S., Woods, S. C., Huypens, P., Beckers, J., de Angelis, M. H., Schürmann, A., Bakhti, M., Klingenspor, M., Heiman, M., Cherrington, A. D., Ristow, M., Lickert, H., Wolf, E., Havel, P. J., Müller, T. D., and Tschöp, M. H. (2018) Animal models of obesity and diabetes mellitus. *Nat. Rev. Endocrinol.* **14**, 140–162
13. Griffen, S. C., Wang, J., and German, M. S. (2001) A genetic defect in beta-cell gene expression segregates independently from the fa locus in the ZDF rat. *Diabetes* **50**, 63–68
14. Cummings, B. P., Bettaieb, A., Graham, J. L., Kim, J., Ma, F., Shibata, N., Stanhope, K. L., Giulivi, C., Hansen, F., Jelsing, J., Vrang, N., Kowala, M., Chouinard, M. L., Haj, F. G., and Havel, P. J. (2013) Bile-acid-mediated decrease in endoplasmic reticulum stress: a potential contributor to the metabolic benefits of ileal interposition surgery in UCD-T2DM rats. *Dis. Model. Mech.* **6**, 443–456
15. Giulivi, C., Ross-Inta, C., Omanska-Klusek, A., Napoli, E., Sakaguchi, D., Barrientos, G., Allen, P. D., and Pessah, I. N. (2011) Basal bioenergetic abnormalities in skeletal muscle from ryanodine receptor malignant hyperthermia-susceptible R163C knock-in mice. *J. Biol. Chem.* **286**, 99–113
16. Huang da, W., Sherman, B. T., and Lempicki, R. A. (2009) Bioinformatics enrichment tools: paths toward the comprehensive functional analysis of large gene lists. *Nucleic Acids Res.* **37**, 1–13
17. Huang da, W., Sherman, B. T., and Lempicki, R. A. (2009) Systematic and integrative analysis of large gene lists using DAVID bioinformatics resources. *Nat. Protoc.* **4**, 44–57
18. Reimand, J., Arak, T., Adler, P., Kolberg, L., Reisberg, S., Peterson, H., and Vilo, J. (2016) g:Profiler-a web server for functional interpretation of gene lists (2016 update). *Nucleic Acids Res.* **44**(W1), W83–W89
19. Breuer, K., Foroushani, A. K., Laird, M. R., Chen, C., Sribnaia, A., Lo, R., Winsor, G. L., Hancock, R. E., Brinkman, F. S., and Lynn, D. J. (2013) InnateDB: systems biology of innate immunity and beyond–recent updates and continuing curation. *Nucleic Acids Res.* **41**(D1), D1228–D1233
20. Kutmon, M., van Iersel, M. P., Bohler, A., Kelder, T., Nunes, N., Pico, A. R., and Evelo, C. T. (2015) PathVisio 3: an extendable pathway analysis toolbox. *PLOS Comput. Biol.* **11**, e1004085
21. Kutmon, M., Riutta, A., Nunes, N., Hanspers, K., Willighagen, E. L., Bohler, A., Mélius, J., Waagmeester, A., Sinha, S. R., Miller, R., Coort, S. L., Cirillo, E., Smeets, B., Evelo, C. T., and Pico, A. R. (2016) WikiPathways: capturing the full diversity of pathway knowledge. *Nucleic Acids Res.* **44**(D1), D488–D494
22. Luo, W., Pant, G., Bhavnasi, Y. K., Blanchard, S. G., Jr., and Brouwer, C. (2017) Pathview Web: user friendly pathway visualization and data integration. *Nucleic Acids Res.* **45**(W1), W501–W508
23. Napoli, E., Song, G., Panoutsopoulos, A., Riyadh, M. A., Kaushik, G., Halmai, J., Levenson, R., Zarbalis, K. S., and Giulivi, C. (2018) Beyond autophagy: a novel role for autism-linked Wdfy3 in brain mitophagy. *Sci. Rep.* **8**, 11348
24. Giulivi, C., Zhang, Y. F., Omanska-Klusek, A., Ross-Inta, C., Wong, S., Hertz-Picciotto, I., Tassone, F., and Pessah, I. N. (2010) Mitochondrial dysfunction in autism. *JAMA* **304**, 2389–2396
25. Napoli, E., Ross-Inta, C., Wong, S., Hung, C., Fujisawa, Y., Sakaguchi, D., Angelastro, J., Omanska-Klusek, A., Schoenfeld, R., and Giulivi, C. (2012) Mitochondrial dysfunction in Pten haplo-insufficient mice with social deficits and repetitive behavior: interplay between Pten and p53. *PLoS One* **7**, e42504
26. Sengupta, P. (2013) The laboratory rat: relating its age with human's. *Int. J. Prev. Med.* **4**, 624–630
27. Gressner, A. M., and Weiskirchen, R. (2006) Modern pathogenetic concepts of liver fibrosis suggest stellate cells and TGF-beta as major players and therapeutic targets. *J. Cell. Mol. Med.* **10**, 76–99
28. She, H., Xiong, S., Hazra, S., and Tsukamoto, H. (2005) Adipogenic transcriptional regulation of hepatic stellate cells. *J. Biol. Chem.* **280**, 4959–4967
29. Tsukamoto, H. (2005) Adipogenic phenotype of hepatic stellate cells. *Alcohol. Clin. Exp. Res.* **29** (11Suppl), 132S–133S
30. Hou, W., and Syn, W. K. (2018) Role of metabolism in hepatic stellate cell activation and fibrogenesis. *Front. Cell Dev. Biol.* **6**, 150
31. Gonzalvez, F., D'Aurelio, M., Boutant, M., Moustapha, A., Puech, J. P., Landes, T., Arnauné-Pelloquin, L., Vial, G., Taleux, N., Slomianny, C., Wanders, R. J., Houtkooper, R. H., Bellenguer, P., Møller, I. M., Gottlieb, E., Vaz, F. M., Manfredi, G., and Petit, P. X. (2013) Barth syndrome: cellular compensation of mitochondrial dysfunction and apoptosis inhibition due to changes in cardiolipin remodeling linked to tafazzin (TAZ) gene mutation. *Biochim. Biophys. Acta* **1832**, 1194–1206
32. Napoli, E., Song, G., Wong, S., Hagerman, R., and Giulivi, C. (2016) Altered bioenergetics in primary dermal fibroblasts from adult carriers of the FMR1 premutation before the onset of the neurodegenerative disease fragile X-associated tremor/ataxia syndrome. *Cerebellum* **15**, 552–564
33. Hatefi, Y. (1985) The mitochondrial electron transport and oxidative phosphorylation system. *Annu. Rev. Biochem.* **54**, 1015–1069
34. Rossignol, R., Gilkerson, R., Aggeler, R., Yamagata, K., Remington, S. J., and Capaldi, R. A. (2004) Energy substrate modulates mitochondrial structure and oxidative capacity in cancer cells. *Cancer Res.* **64**, 985–993
35. Ahmadian, M., Suh, J. M., Hah, N., Liddle, C., Atkins, A. R., Downes, M., and Evans, R. M. (2013) PPARγ signaling and metabolism: the good, the bad and the future. *Nat. Med.* **19**, 557–566
36. Yamauchi, T., Kamon, J., Ito, Y., Tsuchida, A., Yokomizo, T., Kita, S., Sugiyama, T., Miyagishi, M., Hara, K., Tsunoda, M., Murakami, K., Ohteki, T., Uchida, S., Takekawa, S., Waki, H., Tsuno, N. H., Shibata, Y., Terauchi, Y., Froguel, P., Tobe, K., Koyasu, S., Taira, K., Kitamura, T., Shimizu, T., Nagai, R., and Kadowaki, T. (2003) Cloning of adiponectin receptors that mediate antidiabetic metabolic effects. *Nature* **423**, 762–769; erratum: 431, 1123
37. Thakur, V., Pritchard, M. T., McMullen, M. R., and Nagy, L. E. (2006) Adiponectin normalizes LPS-stimulated TNF-alpha production by rat Kupffer cells after chronic ethanol feeding. *Am. J. Physiol. Gastrointest. Liver Physiol.* **290**, G998–G1007
38. Matsunami, T., Sato, Y., Ariga, S., Sato, T., Kashimura, H., Hasegawa, Y., and Yukawa, M. (2010) Regulation of oxidative stress and inflammation by hepatic adiponectin receptor 2 in an animal model of nonalcoholic steatohepatitis. *Int. J. Clin. Exp. Pathol.* **3**, 472–481
39. Tomita, K., Oike, Y., Teratani, T., Taguchi, T., Noguchi, M., Suzuki, T., Mizutani, A., Yokoyama, H., Irie, R., Sumimoto, H., Takayanagi, A., Miyashita, K., Akao, M., Tabata, M., Tamiya, G., Ohkura, T., and Hibi, T. (2008) Hepatic AdipoR2 signaling plays a protective role against progression of nonalcoholic steatohepatitis in mice. *Hepatology* **48**, 458–473
40. Yadav, H., Devalaraja, S., Chung, S. T., and Rane, S. G. (2017) TGF-β1/Smad3 pathway targets PP2a-AMPK-FoxO1 signaling to regulate hepatic gluconeogenesis. *J. Biol. Chem.* **292**, 3420–3432
41. Yuan, N., Zhang, H. F., Wei, Q., Wang, P., and Guo, W. Y. (2018) Expression of CD4+CD25+Foxp3+ regulatory T cells, interleukin 10 and transforming growth factor β in newly diagnosed type 2 diabetic patients. *Exp. Clin. Endocrinol. Diabetes* **126**, 96–101
42. Qiao, Y. C., Chen, Y. L., Pan, Y. H., Ling, W., Tian, F., Zhang, X. X., and Zhao, H. L. (2017) Changes of transforming growth factor beta 1 in patients with type 2 diabetes and diabetic nephropathy: a PRISMA-compliant systematic review and meta-analysis. *Medicine (Baltimore)* **96**, e6583
43. Pscherer, S., Freude, T., Forst, T., Nussler, A. K., Braun, K. F., and Ehnert, S. (2013) Anti-diabetic treatment regulates pro-fibrotic TGF-β serum levels in type 2 diabetics. *Diabetol. Metab. Syndr.* **5**, 48
44. Wobser, H., Dorn, C., Weiss, T. S., Amann, T., Bollheimer, C., Büttner, R., Schölmerich, J., and Hellerbrand, C. (2009) Lipid accumulation in hepatocytes induces fibrogenic activation of hepatic stellate cells. *Cell Res.* **19**, 996–1005
45. Zhang, C. Y., Yuan, W. G., He, P., Lei, J. H., and Wang, C. X. (2016) Liver fibrosis and hepatic stellate cells: etiology, pathological hallmarks and therapeutic targets. *World J. Gastroenterol.* **22**, 10512–10522

46. Lanthier, N., Horsmans, Y., and Leclercq, I. A. (2009) The metabolic syndrome: how it may influence hepatic stellate cell activation and hepatic fibrosis. *Curr. Opin. Clin. Nutr. Metab. Care* **12**, 404–411
47. Sugimoto, R., Enjoji, M., Kohjima, M., Tsuruta, S., Fukushima, M., Iwao, M., Sonta, T., Kotoh, K., Inoguchi, T., and Nakamuta, M. (2005) High glucose stimulates hepatic stellate cells to proliferate and to produce collagen through free radical production and activation of mitogen-activated protein kinase. *Liver Int.* **25**, 1018–1026
48. Gupta, S., Stravitz, R. T., Dent, P., and Hylemon, P. B. (2001) Down-regulation of cholesterol 7alpha-hydroxylase (CYP7A1) gene expression by bile acids in primary rat hepatocytes is mediated by the c-Jun N-terminal kinase pathway. *J. Biol. Chem.* **276**, 15816–15822
49. Vlahcevic, Z. R., Eggertsen, G., Björkhem, I., Hylemon, P. B., Redford, K., and Pandak, W. M. (2000) Regulation of sterol 12alpha-hydroxylase and cholic acid biosynthesis in the rat. *Gastroenterology* **118**, 599–607
50. Shi, X., Burkart, A., Nicoloro, S. M., Czech, M. P., Straubhaar, J., and Corvera, S. (2008) Paradoxical effect of mitochondrial respiratory chain impairment on insulin signaling and glucose transport in adipose cells. *J. Biol. Chem.* **283**, 30658–30667
51. Andrzejewski, S., Gravel, S. P., Pollak, M., and St-Pierre, J. (2014) Metformin directly acts on mitochondria to alter cellular bioenergetics. *Cancer Metab.* **2**, 12
52. Saisho, Y. (2015) Metformin and inflammation: its potential beyond glucose-lowering effect. *Endocr. Metab. Immune Disord. Drug Targets* **15**, 196–205
53. Woo, S. L., Xu, H., Li, H., Zhao, Y., Hu, X., Zhao, J., Guo, X., Guo, T., Botchlett, R., Qi, T., Pei, Y., Zheng, J., Xu, Y., An, X., Chen, L., Chen, L., Li, Q., Xiao, X., Huo, Y., and Wu, C. (2014) Metformin ameliorates hepatic steatosis and inflammation without altering adipose phenotype in diet-induced obesity. *PLoS One* **9**, e91111
54. Houtkooper, R. H., and Vaz, F. M. (2008) Cardiolipin, the heart of mitochondrial metabolism. *Cell. Mol. Life Sci.* **65**, 2493–2506
55. Osman, C., Voelker, D. R., and Langer, T. (2011) Making heads or tails of phospholipids in mitochondria. *J. Cell Biol.* **192**, 7–16
56. Gohil, V. M., Hayes, P., Matsuyama, S., Schägger, H., Schlame, M., and Greenberg, M. L. (2004) Cardiolipin biosynthesis and mitochondrial respiratory chain function are interdependent. *J. Biol. Chem.* **279**, 42612–42618
57. Gohil, V. M., and Greenberg, M. L. (2009) Mitochondrial membrane biogenesis: phospholipids and proteins go hand in hand. *J. Cell Biol.* **184**, 469–472
58. Pfeiffer, K., Gohil, V., Stuart, R. A., Hunte, C., Brandt, U., Greenberg, M. L., and Schägger, H. (2003) Cardiolipin stabilizes respiratory chain supercomplexes. *J. Biol. Chem.* **278**, 52873–52880
59. Duthie, S. J., Ma, A., Ross, M. A., and Collins, A. R. (1996) Antioxidant supplementation decreases oxidative DNA damage in human lymphocytes. *Cancer Res.* **56**, 1291–1295
60. Duthie, S. J., Narayanan, S., Blum, S., Pirie, L., and Brand, G. M. (2000) Folate deficiency *in vitro* induces uracil misincorporation and DNA hypomethylation and inhibits DNA excision repair in immortalized normal human colon epithelial cells. *Nutr. Cancer* **37**, 245–251

Received for publication December 14, 2018.
Accepted for publication June 25, 2019.